Valence band electronic structure characterization of the rutile TiO_2 (110)-(1×2) reconstructed surface

C. Sánchez-Sánchez [a,b], M.G. Garnier [c], P. Aebi [c], M. Blanco-Rey [d], P.L. de Andres [a,d], J.A. Martín-Gago [a,e], M.F. López [a,*]

[a] Instituto Ciencia de Materiales de Madrid (ICMM-CSIC), C/Sor Juana Inés de la Cruz 3, 28049-Madrid, Spain
[b] Instituto de Ciencia de Materiales de Sevilla (ICMSE-CSIC), Américo Vespucio 49, 41092-Sevilla, Spain
[c] Département de Physique and Fribourg Center for Nanomaterials, Université de Fribourg, CH-1700 Fribourg, Switzerland
[d] Donostia International Physics Center, Universidad del País Vasco UPV/EHU, Paseo Manuel de Lardizábal 4, 20018 Donostia-San Sebastián, Spain
[e] Centro de Astrobiologia (CSIC-INTA), 28850 Madrid, Spain

The electronic structure of the TiO_2 (110)-(1×2) surface has been studied by means of angular resolved ultraviolet photoemission spectroscopy (ARUPS). The valence band dispersion along the high symmetry surface directions, [001] and [1–10], has been recorded. The experimental data show no dispersion of the band-gap Ti 3d states. However, the existence of dispersive bands along the [001] direction located at about 7 eV below the Fermi level is reported. The existence of two different contributions in the emission from the defects-related state located in the gap of the surface is univocally shown for the first time.

1. Introduction

Metal oxides are of great importance due to their use in several technological applications such as heterogeneous catalysis, photochemistry, sensors, and composite materials [1]. Among all of them, titanium dioxide has become the prototype for surface science studies due to its ordered structure and its capability of conduction upon reduction. One of the main areas of application of TiO_2 is the field of catalysis, being nowadays one of the more widely used materials for catalytic supports. In order to better understand and improve its catalytic properties, a detailed knowledge of its electronic structure is of crucial importance. The rutile TiO_2 (110) is the most stable face and, in this work, we shall focus on its electronic properties. This surface, upon sputtering and annealing under ultra-high vacuum (UHV) conditions, presents the well-known (1×1) structure corresponding to the bulk truncated structure, modified by simple but relevant surface relaxations [2].

The stable (1×1) surface transforms into a long range ordered structure with (1×2) symmetry upon further reduction of the substrate [3]. The quality of this new surface depends on the reduction level of the TiO_2 crystal, on the annealing temperature achieved during sample preparation, and on the duration of the annealing. This surface reconstruction has been the subject of many investigations during the last years. Most of the scientific efforts have been devoted towards the determination of the geometrical disposition of atoms. This has been a matter of controversy, as several atomic models have been proposed based on different experimental techniques and theoretical calculations [4–9].

In a previous work carried out by our group, the (1×2) structure was elucidated from density functional theory (DFT) calculations and quantitative low-energy electron diffraction experiments [LEED-I(V)] [10,11]. Similar to Onishi's proposal, a Ti_2O_3 stoichiometry on the surface was favored, although some structural differences between these two models were reported. Surprisingly, not many investigations have focused on the electronic structure of the (1×2) surface reconstruction.

One significant issue in the study of TiO_2 is the presence of defects of different nature, which are typical of this kind of substrates. Its importance arises from the fact that the presence of these defects, hydroxyl impurities, oxygen atom vacancies and interstitials Ti atoms, confer unusual properties to this material. The local character of these defects makes near-field scanning probe microscopy a crucial technique for their study, although its assignation is not always clear and straightforward [12–18], not only regarding the surface topography but also from the electronic point of view. Depending on the amount of defects, some can be also detectable by spectroscopic techniques. The oxidation state of titanium cations in stoichiometric (110) TiO_2 corresponds nominally to Ti^{4+}. However, an important contribution of defects will be originated when the surface is reduced by annealing and/or ion bombardment. The presence of these defects, not only mainly oxygen vacancies but also, in a lower amount, interstitials Ti^{3+} atoms, on the TiO_2 (110) surface will lead to an excess of

* Corresponding author. Tel.: +34 91 3349081; fax: +34 91 372 0623.
E-mail address: mflopez@icmm.csic.es (M.F. López).

electrons at these specific sites. This residual charge is expected to be transferred to the Ti atoms located close to defects [19–21].

Consequently, the trapped electron will partially populate the Ti 3d orbitals and will change the oxidation state of the adjacent Ti cations from 4+ to 3+. For this reason, when the defects contribution is high, a new electronic state appears in the gap region below EF. This state is referred in ultraviolet photoemission spectra as band-gap or defects-related state and it has been the subject of many spectroscopic studies [22,23]. Since the TiO_2 (110)-(1×2) surface reconstruction is obtained from the (1×1) surface by annealing at high temperature, a significant amount of defects are originated in this process. Thus, a clear enhancement of the Ti^{3+} band-gap state is expected for the (1×2) reconstruction [24]. Additionally, the presence of surface Ti_2O_3 rows where the Ti cations have a nominal 3+ oxidation state will contribute to enhance the emission at the band-gap state.

In this paper, the valence band electronic structure of the rutile TiO_2 (110)-(1×2) surface is investigated by angular resolved ultraviolet photoemission spectroscopy (ARUPS). Special effort has been made to understand the origin of the band-gap state that appears at a binding energy (BE) of approximately 0.9 eV. We will show that for the (1×2) reconstruction this peak presents a double contribution, one associated to the Ti^{3+} in the Ti_2O_3 rows of the (1×2) reconstruction, and a different one related to the defective Ti^{3+} atoms present throughout the crystal bulk. We also report the presence of a dispersive band at a BE of about 7 eV and $k// = 0.35$ $Å^{-1}$.

2. Material and methods

Experiments have been carried out in two different ultra-high vacuum (UHV) chambers, both of them with a base pressure better than $1 \cdot 10^{-10}$ mbar. In both cases, a commercial rutile TiO_2 (110) sample (Mateck) was prepared through repeated cycles of sputtering and annealing at 1150 K until a sharp (1×1) or (1×2) LEED pattern was obtained. The (1×1) surface is characteristic of a stoichiometric sample or a poorly reduced bulk, while the (1×2) reconstruction is typical of heavily reduced substrates. For the UPS band-gap peak study, three different substrates were considered: low, medium and heavily reduced. The criteria used to discern among these three cases have been the color of the sample and the surface structure. In this way, for example, low reduced sample presents a light blue color and a (1×1) surface structure (as observed by STM and LEED). Medium reduced sample is dark blue but still with a (1×1) surface structure. Finally, heavily reduced sample is almost black and presents a (1×2) surface termination. In all cases the same sample was used, and the degree of reduction was increased by controlling the annealing temperature and the cycle duration. ARUPS measurements were performed using monochromatized He-I radiation from a He discharge lamp in combination with a VG EscaLab Mk II photoelectron spectrometer (20 meV resolution), and a sample goniometer for full hemispherical Angular Resolved Photoemission Spectroscopy (ARPES) [25]. The angular acceptance and resolution is 1° full-cone. Therefore, this corresponds to an approximate kII integration of the Brillouin zone of less than 0.04 $Å^{-1}$. Measurements of the band-gap state were done at the UHV chamber located at Centro de Astrobiología (CSIC-INTA), equipped with a hemispherical electron analyzer and a He-I lamp. To perform the ultraviolet photoemission spectroscopy (UPS) analysis the spectra were fitted to a least squares combination of Gaussian components. The background selected for the fitting procedure of the UPS spectra was a linear one as it is the typical used for inelastic backgrounds without a stepwise change in intensity, as it was our case. All spectra were recorded at room temperature.

The (1×2) reconstructed Ti_2O_3 surface structure was determined from DFT and dynamical LEED in a previous work [10], and the surface model in the present paper has been constructed accordingly. The (1×2) supercell lattice dimensions are a = 13.22 Å, b = 2.99 Å, and c = 3a, containing a slab of 70 atoms mirror-symmetric about its middle plane, exposing the Ti_2O_3 reconstruction at both sides (see supplementary information). This ensures that the electronic structure features come only from the bulk and the (1×2) reconstructed surface. The TiO_2 bulk unit cell dimensions are a = b = 4.68 Å and c = 2.99 Å. The plane wave basis has been constructed with a cut-off energy of 400 eV and a Monkhorst-Pack k-point mesh of 7×13×1 (4×4×7 for bulk) [26]. Energy was converged up to 0.01 meV/ion and the Fermi level to 0.001 meV/ion. The supercell height, c, is such that the solid occupies approximately one half of the supercell, which we have shown to be enough to avoid interactions between consecutive slabs. The slab thickness is such that Mulliken charges of atoms in the central Ti–O layer are in good agreement with those of the bulk. The outmost 19 atoms of both sides of the slab were allowed to relax further with tolerances of 0.05 eV/Å in the force per atom and 0.001 Å in the displacement. The final atomic coordinates differed from those of the previous work [10] by no more than 0.04 Å. Actual calculations have been performed with the CASTEP code [29].

3. Results and discussion

Fig. 1(a) shows a schematic representation of the atomic arrangement corresponding to the rutile TiO_2 (110)-(1×2) surface reconstruction, as derived from previous LEED I(V) and DFT calculations [10]. The most protruding features on this surface are the Ti_2O_3 rows, which extend along the [001] direction. Large gray and small red circles correspond to Ti and O atoms, respectively. Ti^{3+} atoms associated to the surface reconstruction are marked by arrows. The red rectangle of Fig. 1(b) represents the surface Brillouin zone (SBZ) for the TiO_2 (110)-(1×2) termination, with the two high-symmetry directions indicated. In this representation also the SBZ for the TiO_2 (110)-(1×1) surface is exhibited as a black rectangle. As it can be observed, both the (1×1) and the (1×2) surfaces present a rectangular structure in the reciprocal space.

Fig. 2(a) and (b) exhibits bidimensional representations of the experimental ARUPS spectra corresponding to the rutile TiO_2 (110)-(1×2) valence band as a function of the momentum parallel component k II along [001] and [1–10] directions, respectively. In both graphs, the high symmetry points of the SBZ as well as the Fermi surface edge are indicated. In the images, the darkest features correspond to more intense photoemission peaks while the brightest ones represent the less intense emissions. Along the [001] direction, i.e. the direction of the Ti_2O_3 rows, a convex dispersive band located at a binding energy of about 7 eV and centered at 0.35 $Å^{-1}$ can be observed. On the other hand, no dispersion is observed along the [1–10] direction, i.e. perpendicular to the reconstruction rows. Previous results on TiO_2 (110)-(1×1) showed weak dispersion of the states corresponding to the valence band [27].

Fig. 2(c) and (d) shows the bidimensional representations of the experimental band-gap state ARUPS spectra along the two high symmetry directions, [001] and [1–10], respectively. The data indicate that no dispersion can be distinguished by ARUPS. In particular, from Fig. 2(c), we conclude there is no significative experimental dispersion of the band-gap state of the (1×2) surface along the direction of the Ti_2O_3 surface wires. This result contrasts with the theoretical prediction derived from DFT calculations about the metallic character of the Ti_2O_3 chains along the [001] direction [10]. This discrepancy has been associated to the tendency of the GGA functional [30] to overestimate the delocalization of states that may be otherwise localized by different factors, like correlation effects and the quasi-1D character of states running along the reconstruction chains. Indeed, the use of GGA + U as an alternative exchange and correlation functional favors the opening of a gap along the [001] direction and results in a dispersive state in the band gap, localized at the subsurface Ti atoms in the trenches between the Ti_2O_3 chains [31,32]. Fig. 3 shows the computed valence band electronic structure for a slab (left) and the corresponding projection of bulk states along the GΓ–Z direction (right).

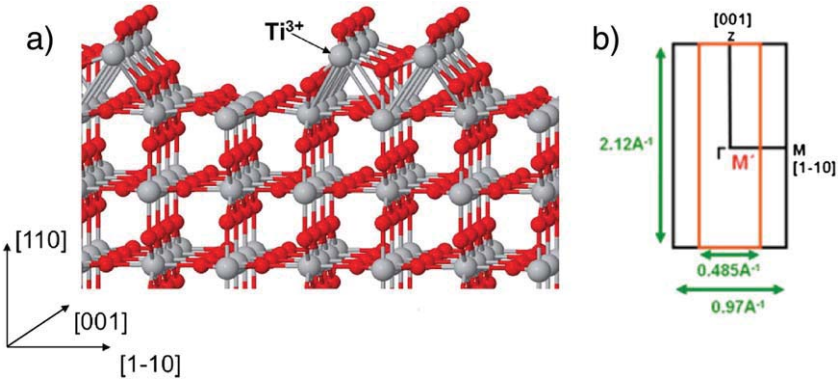

Fig. 1. a) Schematic representation of the atomic arrangement corresponding to the (1×2) TiO_2 (110) surface reconstruction as inferred from DFT calculations (only the last layers are shown). Large (blue) and small circles (red) correspond to Ti and O atoms, respectively. b) Surface Brillouin zone for the TiO_2 (110)-(1×2) surface reconstruction marked in red with the two high-symmetry directions [001] and [1–10]. The black rectangle corresponds to the extended SBZ for TiO_2 (110)-(1×1) surface. (For interpretation of the references to color in this figure legend, the reader is referred to the web version of this article.)

Blue dots label states with more than an 80% contribution from atoms of the Ti_2O_3 chains, while green dots represent the same for atoms located on the TiO_2 tri-layer closest to the surface. As it is well known, DFT underestimates the band gap because correlation effects are only taken into account in an approximate way (we obtain for bulk TiO_2 a band gap of 2 eV). Furthermore, the Hohenberg–Kohn theorem applies strictly speaking only to the ground state, and excited states, e.g. in the conduction band, are only covered in an approximate, perturbative way. Finally, the ARUPS technique only provides information about the valence band. Therefore, we only attempt to compare the experimental and theoretical valence bands. In the right hand side panel of Fig. 3 we show the bands along the G–Z direction from a bulk only calculation (i.e. from the 1×1×1 bulk unit cell for TiO_2, as described above). We compare the bulk states from this calculation with the experimental ones in Fig. 2a. It is interesting to notice that these states are not affected by the low-dimensional comments made above for the Ti_2O_3 chains, and are therefore properly described by a GGA functional. This point is double-checked by performing LDA + U calculations (U = 4.5 eV); the main effect is a rigid shift of bands by about half an eV to higher binding energies, but no noticeable distortions. The main observed features appear above and below 7 eV, similarly as can be seen in the experiment (panel (a) in Fig. 2). On the other hand, the states related to the surface (green triangles and circles) show a remarkable lack of dispersion very near 7 eV. The experimental resolution does not allow seeing this flat surface-like band. For the experimental band structure, a dispersive band similar to the theoretical one happens above and below 7 eV, as seen by comparing with Fig. 2 (panel a).

Finally, we notice in Fig. 2(c) and (d), that the data exhibit intensity maxima at approximately 0.8 $Å^{-1}$ (along [001]) and 0.15 $Å^{-1}$ (along [1–10]). This can be explained by final-state scattering effects, i.e. as an ultraviolet photoelectron diffraction effect (UPD) [28].

In order to extract additional information on the band-gap states, UPS measurements for three different reduction levels of the substrate have been performed. As it has been mentioned above, it is known that the band-gap state is related to Ti^{3+} states and it appears after bulk reduction. However, in the case of the (1×2) surface reconstruction, there are also Ti^{3+} states associated to the Ti_2O_3 rows of the

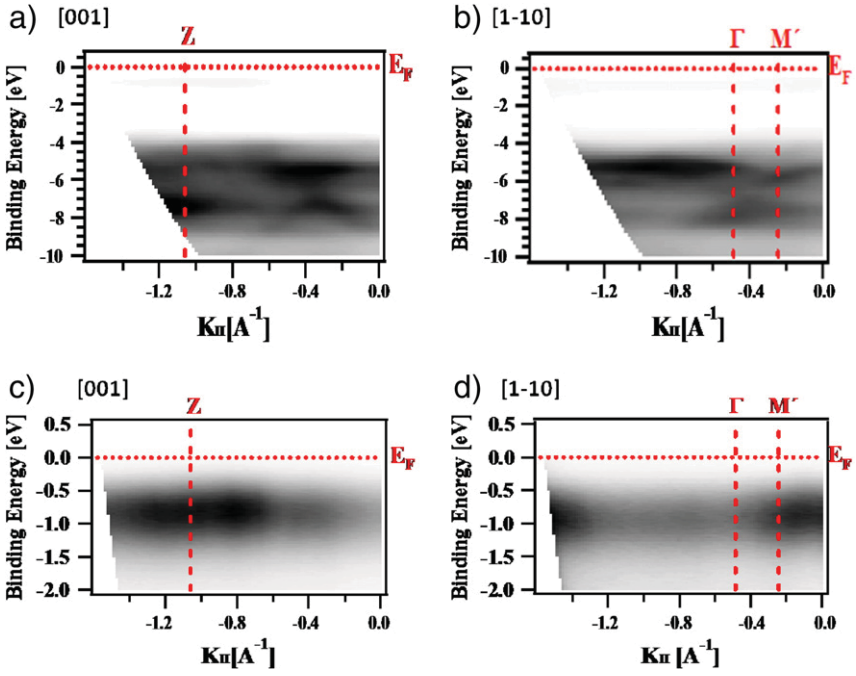

Fig. 2. Bidimensional representation of the ARUPS spectra of the TiO_2 (110)-(1×2) surface as a function of k II along (a) [001] and (b) [1–10] directions for the valence band region, and (c) and (d) for the band-gap states region along [001] and [1–10], respectively.

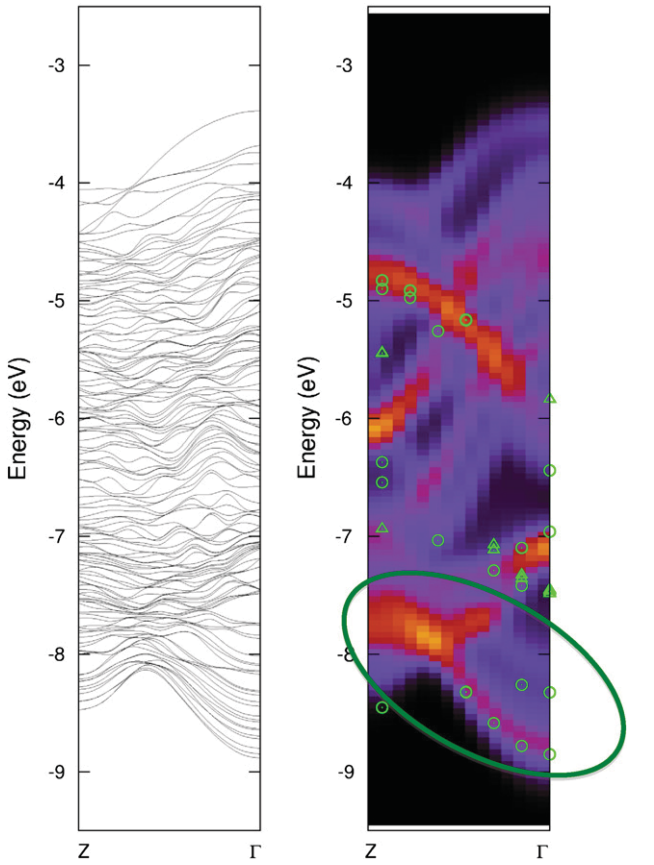

Fig. 3. Ab-initio DFT electronic structure calculation along the [001] direction (G–Z). (i) Left panel: band structure of the slab supercell (with the Ti_2O_3 1×2 reconstructed chains). (ii) Right panel: band structure of the $1\times1\times1$ bulk TiO_2 unit cell projected along the G–Z direction. Red regions in the graph correspond to bulk states with a large weight in the projection along the G–Z direction. Blue and violet correspond to states with small weight and black regions are either gaps or zones with a very small number of states. Green triangles label electronic states that have more than 80% contribution from atoms in the Ti_2O_3 group, as obtained in the left panel. Green circles label the same corresponding to atoms of the topmost trilayer (TiO_2). Green ellipse marks the dispersive band similar to the experimental one. (For interpretation of the references to color in this figure legend, the reader is referred to the web version of this article.)

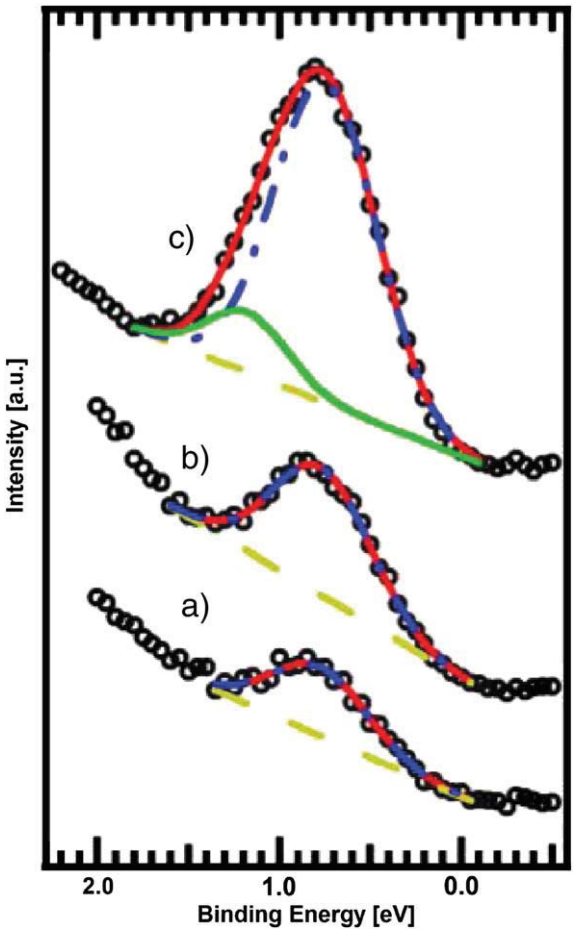

Fig. 4. UPS spectra of the band-gap states region for: (a) poorly reduced substrate with a (1×1) surface, (b) highly reduced substrate with (1×1) symmetry at the surface, and (c) heavily reduced substrate with a (1×2) symmetry at the surface. (For interpretation of the references to color in this figure legend, the reader is referred to the web version of this article.)

surface reconstruction. It is generally accepted that the exact binding energy of an electron depends not only on the level from which photoemission originates but also on the oxidation state of the atom and the local chemical environment. Thus, modifications on the local chemical environment introduce small shifts in the peak position, which are known as chemical shifts. In the present case, two different chemical environments for the Ti^{3+} ions are present, one at the bulk and another at the Ti_2O_3 surface rows. For this reason, these two different chemical settings should give rise to different photoemission signals separated by a certain binding energy, making possible their distinction by means of UPS. Fig. 4 exhibits UPS spectra of the band-gap state region for both a poorly reduced and a highly reduced substrate with a (1×1) surface symmetry, and for a heavily reduced substrate with (1×2) symmetry at the surface. In all spectra, the red solid line through the black data circles represents the result of the least-squares fit, with the blue dashed-dotted component giving the signal corresponding to the low binding energy (BE) peak and the green solid curve showing the high BE emission. The yellow dashed line represents the linear background. As it can be observed in Fig. 4(a), for a low reduction level associated to a TiO_2 (110)-(1×1) surface, just one peak is needed in order to properly fit the experimental data (chi-square test is 0.079). The binding energy for this peak is 0.78 eV with a FWHM value of 0.62 eV. If the reduction level is increased (but still preserving a (1×1) surface) an enhancement of the band-gap state is observed, as it is evident from Fig. 4(b). Again, only one peak is necessary to fit the experimental data, being this peak almost identical to the previous one, except for an increase in its intensity. In this case, its binding energy is 0.77 eV and the FWHM is 0.63 eV (chi-square 0.047). On the other hand, upon further reduction of the substrate a phase transition takes place at the surface, where a new reconstruction appears as it is evidenced from LEED and STM measurements. This new reconstruction, characterized by a Ti_2O_3 surface stoichiometry, presents a wider and asymmetric band-gap state peak, which makes necessary the addition of a second component in the fit. Indeed, for the heavily reduced substrate with a (1×2) surface termination, two contributions have been required to properly fit the band-gap state emission, one located at the same position as in the previous cases, and another one located at a slightly higher BE (Fig. 4(c)). The two curves used in these fits are located at 0.75 eV and 1.18 eV BE showing a FWHM of 0.67 eV and 0.51 eV, respectively (chi-square 0.077). Attempts to fit this spectrum with a single component have been unsuccessful due to the asymmetry of the experimental data (best chi-square obtained has been 0.43). This new state appearing together with the (1×2) surface reconstruction and not observed for any of the (1×1) symmetry cases, can only be associated to the Ti^{3+} states of the Ti_2O_3 rows. As it would be expected from the existence of two different chemical environments associated with the Ti^{3+} states, the UPS experiments clearly indicate the presence of two different contributions in the band-gap state peak: one component is related to the bulk defects typical of the (1×1) structure

(low BE peak), and the other is due to the Ti atoms present at the surface reconstruction in the (1×2) surface (high BE peak). The presence of this new surface termination in the (1×2) TiO_2 (110) sample surface, i.e. the Ti_2O_3 surface rows, is the origin of the sudden appearance of the latter component. It is important to note the increase in the intensity of the peak at 0.75 eV for this sample in comparison to the less reduced ones. The reason of this effect is the increasing amount of Ti^{3+} states not only at the Ti_2O_3 surface rows (peak at 1.18 eV BE) but also at the bulk (peak at 0.75 eV BE) when the sample has been reduced.

It is worthy to comment on the different contexts for Ti^{3+} and Ti^{4+} atoms in the (1×2) TiO_2 (110) sample. The geometrical disposition of the Ti^{3+} atoms at the surface within the Ti_2O_3 chains, and therefore its chemical environment, is completely different to that of the of Ti^{3+} atoms at the bulk near the defect sites. However, in the case of the Ti^{4+} atoms, the geometrical arrangement in both cases, bulk and surface, is the same. For this reason, no shift in the binding energies should be expected for the surface Ti^{4+} atoms.

The possibility of discerning the two components for the band-gap states peak leads to some important consequences. For example, this method based on fitting the bad-gap states region can be used to confirm the existence and quality level of the (1×2) surface reconstruction on TiO_2(110). It could be also used to determine the nature of the interaction of a molecular adsorbate on the (1×2) reconstruction by analyzing the evolution of the relative intensity of the different components of the band-gap state peak upon deposition.

4. Conclusions

In this paper, the electronic structure of the rutile TiO_2 (110)-(1×2) surface reconstruction has been characterized, paying special attention to Ti^{3+} related band-gap state. By means of ARUPS, the presence of a downward dispersive band along the rutile TiO_2 (110)-(1×2) [001] surface direction is determined. This band, with its maximum at 0.35 $Å^{-1}$, appears 7 eV below the Fermi edge. No dispersion of the band-gap states is observed by ARUPS. Regarding the band-gap states emission, the double nature of this peak has been identified. One component is associated to the Ti^{3+} cations next to the bulk defects and the other, observed for the case of the TiO_2 (110)-(1×2) surface reconstruction, to the Ti^{3+} cations in the Ti_2O_3 chains present at the surface.

Acknowledgments

This work has been supported by the Spanish CYCIT (MAT2011-26534) and the Ministry of Science and Innovation (CSD2007-41 NANOSELECT). C.S.S. gratefully acknowledges Ministerio de Educación for the financial support inside the "FPU programme" under the AP2005-0433 grant. M.G. G. and P.A. are grateful for the support by the Fonds National Suisse pour la Recherche Scientifique through Div. II and the Swiss National Center of Competence in Research MaNEP. M.B.-R. acknowledges financial support from the Gipuzkoako Foru Aldundia and the European Union 7th Framework Programme (FP7/2007–2013) under grant agreement no. FP7-PEOPLE-2010-RG276921.

Appendix A. Supplementary data

Supplementary data to this article can be found online at http://dx.doi.org/10.1016/j.susc.2012.09.019.

References

[1] U. Diebold, Surf. Sci. Rep. 48 (2003) 53.
[2] W. Busayaporn, X. Torrelles, A. Wander, S. Tomić, A. Ernst, B. Montanari, N.M. Harrison, O. Bikondoa, I. Joumard, J. Zegenhagen, G. Cabailh, G. Thornton, R. Lindsay, Phys. Rev. B 81 (2010) 153404 (and references therein).
[3] J. Abad, C. Rogero, J. Méndez, M.F. López, J.A. Martín-Gago, E. Román, Surf. Sci. 600 (2006) 2696.
[4] P.J. Møller, M.C. Wu, Surf. Sci. 224 (1989) 265.
[5] H. Onishi, K.I. Fukui, Y. Iwasawa, Bull. Chem. Soc. Jpn. 68 (1995) 2447.
[6] C.L. Pang, S.A. Haycock, H. Raza, P.W. Murray, G. Thornton, O. Gülseren, R. James, D.W. Bullet, Phys. Rev. B 58 (1998) 1586.
[7] R.A. Bennett, P. Stone, N.J. Price, M. Bowker, Phys. Rev. Lett. 82 (1999) 3831.
[8] K.T. Park, M.H. Pan, V. Meunier, E.W. Plummer, Phys. Rev. Lett. 96 (2006) 226105.
[9] N. Shibata, A. Goto, S.-Y. Choi, T. Mizoguchi, S.D. Findlay, T. Yamamoto, Y. Ikuhara, Science 322 (2008) 570.
[10] M. Blanco-Rey, J. Abad, C. Rogero, J. Mendez, M.F. Lopez, J.A. Martin-Gago, P.L. de Andres, Phys. Rev. Lett. 96 (2006) 055502.
[11] M. Blanco-Rey, J. Abad, C. Rogero, J. Méndez, M.F. López, E. Román, J.A. Martín-Gago, P.L. de Andrés, Phys. Rev. B 75 (2007) 081402(R).
[12] J.V. Lauritsen, A.S. Foster, G.H. Olesen, M.C. Christensen, A. Kühnle, S. Helveg, J.R. Rostrup-Nielsen, B.S. Clausen, M. Reichling, F. Besenbacher, Nanotechnology 17 (2006) 3436.
[13] X. Cui, Z. Wang, S. Tan, B. Wang, J. Yang, J.G. Hou, J. Phys. Chem. C 113 (2009) 13204.
[14] C.L. Pang, O. Bikondoa, D.S. Humphrey, A.C. Papageorgiou, G. Cabailh, R. Ithnin, Q. Chen, C.A. Muryn, H. Onishi, G. Thornton, Nanotechnology 17 (2006) 5397.
[15] C. Sánchez-Sánchez, C. González, P. Jelinek, J. Méndez, P.L. de Andrés, J.A. Martín-Gago, M.F. López, Nanotechnology 21 (2010) 405702.
[16] A. Yurtsever, Y. Sugimoto, M. Abe, S. Morita, Nanotechnology 21 (2010) 165702.
[17] R. Bechstein, C. González, J. Schütte, P. Jelínek, R. Pérez, A. Kühnle, Nanotechnology 20 (2009) 505703.
[18] H.P. Pinto, G.H. Enevoldsen, F. Besenbacher, J.V. Lauritsen, A.S. Foster, Nanotechnology 20 (2009) 264020.
[19] P. Krüger, S. Bourgeois, B. Domenichini, H. Magnan, D. Chandesris, P. Le Fèvre, A.M. Flank, J. Jupille, L. Floreano, A. Cossaro, A. Verdini, A. Morgante, Phys. Rev. Lett. 100 (2008) 055501.
[20] M. Nolan, S.D. Elliott, J.S. Mulley, R.A. Bennett, M. Basham, P. Mulheran, Phys. Rev. B 77 (2008) 235424.
[21] M.V. Ganduglia-Pirovano, A. Hofmann, J. Sauer, Surf. Sci. Rep. 62 (2007) 219.
[22] R. Patel, Q. Guo, I. Coks, E.M. Williams, E. Roman, J.L. de Segovia, J. Vac. Sci. Technol. A 15 (1997) 2553.
[23] Z. Zhang, S. Jeng, V.E. Henrich, Phys. Rev. B 43 (1991) 12004.
[24] J. Abad, C. Rogero, J. Méndez, M.F. López, J.A. Martín-Gago, E. Román, Appl. Surf. Sci. 234 (2004) 497.
[25] T. Pillo, L. Patthey, E. Boschung, J. Hayoz, P. Aebi, L. Schlapbach, J. Electron Spectrosc. Relat. Phenom. 97 (1998) 243.
[26] H.J. Monkhorst, J.D. Pack, Phys. Rev. B 13 (1976) 5188.
[27] S. Fischer, J.A. Martín-Gago, E. Román, K.D. Schierbaum, J.L. de Segovia, J. Electron Spectrosc. Relat. Phenom. 83 (1997) 217.
[28] J. Osterwalder, T. Greber, P. Aebi, R. Fasel, L. Schlapbach, Phys. Rev. B 53 (1996) 10209.
[29] S. Clark, M. Segall, C. Pickard, P. Hasnip, M. Probert, K. Refson, M.C. Payne, Z. Kristallogr. 220 (2005) 570 (http://www.accelrys.com).
[30] J.P. Perdew, K. Burke, M. Ernzerhof, Phys. Rev. Lett. 77 (1996) 3865.
[31] V. Celik, H. Unal, E. Mete, S. Ellialtioglu, Phys. Rev. B 82 (2010) 205113.
[32] H. Unal, E. Mete, S. Ellialtioglu, Phys. Rev. B 84 (2011) 115407.